Macromolecules
ARTICLE

Macromolecules **2010**, *43*, 1583–1591 **1583**
DOI: 10.1021/ma902060k

Mesoscale Molecular Dynamics Simulations of the Force between Surfaces with Grafted Poly(ethylene oxide) Chains Derived from Atomistic Simulations

Rodrigo M. Cordeiro,[†] Florian Zschunke,[‡] and Florian Müller-Plathe*,[†]

[†]*Physikalische Chemie, Technische Universität Darmstadt, Petersenstrasse 20, D-64287, Darmstadt, Germany and* [‡]*Evonik Degussa GmbH, Rodenbacher Chaussee 4, D-63457, Hanau, Germany*

Received September 16, 2009; Revised Manuscript Received December 16, 2009

ABSTRACT: The force between parallel surfaces with grafted poly(ethylene oxide) chains was calculated using molecular dynamics simulations. First, a single chain surrounded by water molecules was simulated with full atomistic detail. On the basis of that, a coarse-grained model with implicit solvent was developed. The force between surfaces with grafted coarse-grained chains was calculated as a function of surface separation (3−18 nm), chain length (12−20 repeat units), grafting density ($\Gamma = 0.01-2.04$ chains/nm^2), and interactions between surface and polymer. Results showed that the force was mainly repulsive and increased monotonically as distance decreased. Chain length had a stronger influence on the force than Γ. For purely repulsive interactions between polymer and surfaces, chains had extended conformations, leading to higher repulsive forces between surfaces. For surfaces with higher affinity for polymer, adsorption took place. The force between surfaces was significant only for high Γ because chains then achieved more extended conformations.

1. Introduction

Poly(ethylene oxide) (PEO), also known as poly(ethylene glycol) (PEG), is a nonionic surfactant that may drastically change the interfacial properties of colloidal particles in aqueous solutions. PEO chains that are either chemically grafted or adsorbed on a surface may increase surface wettability and also hinder particle aggregation by means of steric stabilization. This last effect is of entropic nature. It comes from the fact that chains placed on two surfaces must fold and/or interdigitate as the respective particles come closer. As a result, the energy of activation for aggregation is increased. Because of that, PEO is extensively used in industry to improve particle dispersibility.[1] A deeper understanding of the stabilization mechanism may help to optimize particle coating and minimize the amount of additive needed, leading to lower production costs and reducing environmental impact.[2]

There has been a number of articles devoted to the simulation of the force between surfaces bearing grafted chains,[3−6] with emphasis to the work of Duque et al., which represents a stepping stone toward other systems that are more involved to simulate but with practical interest.[6] Motivated by these facts, we calculated in the present work the force acting between two parallel planar surfaces with grafted PEO chains by means of molecular dynamics (MD) simulations. We investigated the influence of parameters such as chain length, grafting density and the affinity between polymer and surface on the force acting between these surfaces and consequently on colloid stability.

A typical system consisting of chains with 20 repeat units each and two surfaces with grafting density of 1 chain/nm^2, dimensions of 5×5 nm^2 and separated by a distance of 10 nm encloses approximately 2.5×10^4 atoms, from which about one-quarter constitutes polymer and the rest is water. Simulation of such a system with full atomistic detail demands high computational power, most of which is spent just for the simulation of the solvent. In order to circumvent this limitation, we adopted a multiscale approach combining atomistic MD and mesoscale (also known as coarse-grained) MD[7,8] with implicit solvent.[9] The basic idea of coarse-graining is to replace a whole molecular segment (in this particular case the repeat unit of a PEO chain) by a single interaction center. In a structural approach, the effective potential between these interaction centers is adjusted iteratively until the structure (or the ensemble of conformations) of the coarse-grained chain matches the structure of the original chain from atomistic MD. Examples of structural properties used as basis for the coarse-graining process are radial distribution functions of atoms in the chain and the chain's radius of gyration. To improve efficiency, solvent molecules are completely removed and considered only implicitly, meaning that the influence of water molecules on the chain conformation is included in the coarse-grained potential. For the system described above, this means a drastic reduction of the system size to approximately 1000 interaction sites.

In view of this, the following approach was adopted. First, a smaller system consisting of a single chain surrounded by water molecules and without any surface present was simulated with full atomistic detail. The force field employed here was adapted from the extensively studied and validated force field of Smith et al. for 1,2-dimethoxyethane (DME) and PEO in aqueous solutions.[10−17] Structural properties such as the radial distribution function of oxygen atoms in the PEO chains were calculated and used as targets for a coarse-grained model in which each repeat unit of the original chain was replaced by a single "superatom" (see Figure 1) and water was considered implicitly. The interaction potential between superatoms obtained from the coarse-graining process was then employed in the simulation of bigger systems consisting of two parallel surfaces covered by grafted coarse-grained chains in a square array, as illustrated in Figure 2. In these simulations, each surface was treated as a

*Corresponding author. E-mail: f.mueller-plathe@theo.chemie.tu-darmstadt.de.

Published on Web 01/08/2010

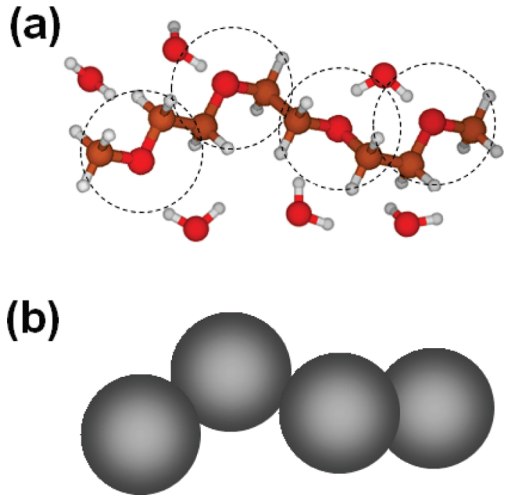

Figure 1. Schematic view of (a) a CH_3-terminated PEO chain surrounded by water and with atomistic detail and (b) its correspondent coarse-grained chain. Orange, red and white beads are C, O and H atoms, respectively. Dashed circles centered at O atoms of the chain backbone represent repeat units mapped as individual superatoms in the coarse-grained model, in which water molecules were considered only implicitly.

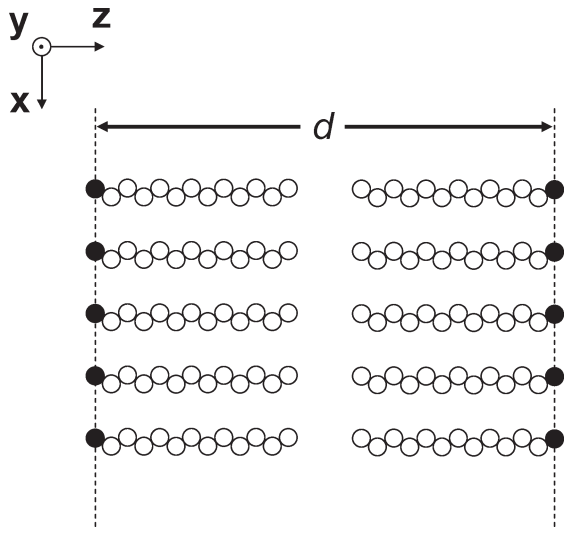

Figure 2. Schematic representation of a typical simulation system constituted by two parallel surfaces (dashed lines) separated by a distance d and with grafted PEO chains, each with 12 coarse-grained repeat units (white circles) and an anchoring element (black circle).

continuum and the force acting between two surfaces was systematically calculated as a function of their separation distance for different values of chain length (12−20 repeat units), grafting density (0.01−2.44 chains/nm^2) and interaction between polymer and surface. These parameters cover a range that is accessible to experiments, as demonstrated by studies using PEO chains with adsorbing head groups on different particles, e.g. sulfur.[1]

2. Simulation Details

2.1. Atomistic Molecular Dynamics. The MD package YASP[18,19] was employed to run all-atom simulations at a pressure of 101.3 kPa (taking into account the potential tail correction) and a temperature of 318 K using a leap-frog integration scheme with a time step of 2 fs. Pressure was controlled using a Berendsen barostat with coupling time $\tau_P = 0.5$ ps and a value of isothermal compressibility of 1.0×10^6 kPa^{-1}. Temperature control was achieved by a Berendsen thermostat with coupling time $\tau_T = 0.2$ ps. The cutoff for nonbonded interactions was $r_c = 0.9$ nm with a Verlet neighbor list cutoff of 1.0 nm updated every 15 steps. The interaction potential V between two nonbonded atoms labeled as i and j at a distance r_{ij} is given as:

$$V_{ij}^{\text{nonbonded}} = 4\varepsilon_{ij}\left(\left[\frac{\sigma_{ij}}{r_{ij}}\right]^{12} - \left[\frac{\sigma_{ij}}{r_{ij}}\right]^{6}\right) + \frac{q_i q_j}{4\pi\varepsilon\varepsilon_0}\left(\frac{1}{r_{ij}} + \frac{\varepsilon_{RF}-1}{2\varepsilon_{RF}+1}\frac{r_{ij}^2}{r_c^3}\right) \quad (1)$$

The first part is a Lennard-Jones potential characterized by the parameters ε_{ij} and σ_{ij}, which are related to the depth of the potential well and the contact distance, respectively. The second part is a Couloumb potential between two charges q_i and q_j in a medium with dielectric constant ε, being ε_0 the vacuum permittivity. The Coulomb term is corrected in order to account for the long-range interactions outside the cutoff. The correction is based on the reaction field model[18] with dielectric constant $\varepsilon_{RF} = 72$, which corresponds to the dielectric constant of pure water at 318 K. In simulations, two atoms were considered as being nonbonded if they belonged to different molecules or if they belonged to the same molecule but were separated by at least two other atoms. Bonded interactions were described by means of harmonic bending energies:

$$V_{ijk}^{\text{angles}} = \frac{1}{2}k_{ijk}^{a}(\theta_{ijk} - \theta_{ijk}^{0})^2 \quad (2)$$

where k_{ijk}^{a} is the angular bending constant, θ_{ijk} is the angle formed by three consecutive atoms and θ_{ijk}^{0} their equilibrium angle. Torsions were given by a sum of cosine functions with different periodicity p:

$$V_{ijkl}^{\text{torsions}} = \sum_{p=1}^{3}\frac{1}{2}k_{ijkl}^{t}\{1 - \cos[p(\varphi_{ijkl} - \varphi_{ijkl}^{0,p})]\} \quad (3)$$

where k_{ijkl}^{t} is the torsional constant, φ_{ijkl} the torsional angle formed by four consecutive atoms and $\varphi_{ijkl}^{0,p}$ the angle in which the energy for each periodicity reaches a minimum.

The systems investigated consisted of a single PEO chain surrounded by ~850 water molecules in a cubic box with lateral dimensions of approximately 3 nm and periodic boundary conditions in all directions. PEO chains had the general formula $R{-}OCH_2{-}(CH_2OCH_2)_{n-2}{-}CH_2O{-}R$, being the terminal group −R either −H or $-CH_3$ and n the total number of repeat units in the chain. The SPC/E force field was employed for water in combination with an adaptation of the extensively studied and validated force field of Smith et al. for DME and CH_3-terminated PEO in aqueous solutions.[10−17] However, in the present work, bonds were considered to be rigid and all bond lengths were kept constant by the SHAKE procedure. Simulations involving H-terminated PEO chains require for the end groups additional parameters that are missing in the original force field of Smith et al., namely those related to the partial charges of the terminal oxygen atom and the hydrogen bounded to it, the O−H bond distance, the H−O−C bond angle and the H−O−C−C and H−O−C−H torsions. These values were obtained from a force field for poly(vinyl alcohol) in water.[20] The partial charges on the remaining H atoms of the terminal monomers were taken as in the force field of Smith et al. and

the charge of the terminal C was adjusted to keep charge neutrality. The parameters adopted for the force field of PEO chains in water are listed in Table 1.

Typical simulation runs consisted of a short *NVT* equilibration period to relax high energy configurations, followed by a *NPT* equilibration step of 10 or 20 ns for chains with 10 or 20 repeat units, respectively. These values are comparable to the relaxation times of chain end-to-end vectors obtained in a previous work for PEO aqueous solutions.[17] Data acquisition at *NPT* for the calculation of average densities, radial distribution functions, radii of gyration, and conformer populations proceeded for the same amount of time used for relaxation.

2.2. Coarse-Grained Molecular Dynamics. Simulations of the coarse-grained systems were performed using a modified version of the MD package IBIsCO.[21] Equations of motion were integrated according to a leapfrog algorithm with a time step of 5 fs. Simulations were performed in the *NVT* ensemble at 318 K using a Berendsen thermostat with coupling time τ_T = 0.05−0.2 ps. Electrostatic interactions were not explicitly considered since they were implicitly included in the coarse-grained nonbonded interactions. A cutoff of 1.3 nm was applied for such interactions with a neighbor list cutoff of 1.4 nm.

In order to build the mesoscopic model, the coarse-grained system was mapped in a way that each superatom was centered at an oxygen atom of the PEO chain backbone and represented a repeat unit of the original chain, as illustrated in Figure 1. Normalized distance and angle distribution functions between consecutive oxygen atoms in the original chain were extracted from atomistic simulations and used as target distribution functions for the coarse-graining procedure. Taking the bond length l between superatoms as an example, multipeaked distributions $P(l)$ were fitted as a sum of m Gaussian functions characterized by their centers (l_{ci}), total area (A_i) and width (w_i):

$$P(l) = \sum_{i=1}^{m} \frac{A_i}{w_i\sqrt{\pi/2}} \exp\left[-2\frac{(l-l_{ci})^2}{w_i^2}\right] \quad (4)$$

The same treatment was applied to the angle distribution function $P(\theta)$. Bonded potentials describing bond stretching and angle bending in coarse-grained systems were then constructed by Boltzmann inversion[7,8] of these target distribution functions, so that:

$$V(l) = -kT \ln P(l) \quad (5)$$

where k is the Boltzmann constant and T the temperature. In the limit of a single Gaussian, this procedure gives rise to harmonic potentials, as demonstrated elsewhere.[8] Gaussian parameters obtained in this way are listed in Table 2.

Nonbonded potentials were constructed in a tabulated form by means of iterative Boltzmann inversion.[7,8] The radial distribution function (RDF) of oxygen atoms separated by at least two other oxygen atoms along the backbone was taken as the target. The process started with a simple Boltzmann inversion of the target RDF to provide an initial guess of the potential (V_0) as a function of distance r. A coarse-grained simulation was run with a tabulated form of the starting potential and the resulting RDF was calculated. The potential of iteration j+1 was then corrected from the potential of the foregoing iteration j according to

$$V_{j+1}(r) = V_j(r) + kT \ln \frac{\mathrm{RDF}_j(r)}{\mathrm{RDF}_{\mathrm{target}}(r)} \quad (6)$$

A new simulation run was performed with the corrected potential and the whole process was repeated until a satisfactory agreement with the target RDF was achieved. The potential obtained by such an iterative process accounts

Table 1. Atomistic Force Field Parameters

Nonbonded Lennard-Jones Parameters

interacting pair[a]	ε [kJ/mol]	σ [nm]
O···C	0.397 67	0.344 77
O···O	0.837 20	0.285 09
H···H	0.041 02	0.300 25
O_w···O_w	0.650 17	0.316 60
C···O	0.577 00	0.313 51
C···H	0.127 72	0.321 74
C···O_w	0.864 41	0.328 17
O···H	0.185 32	0.292 57
O··O_w	1.254 13	0.298 42
H···O_w	0.277 53	0.306 25

Partial Atomic Charges

atom	location	q [e]
C	internal	−0.066
O	internal	−0.256
H	methylene groups	0.097
C	terminal $-CH_3$	−0.163
H	terminal $-CH_3$	0.097
C[b]	terminal $-CH_2OH$	0.106
O[b]	terminal −OH	−0.7
H[b]	terminal −OH	0.4
O_w	water	−0.8476
H_w	water	0.4238

Bond Lengths

bond	length [nm]
C−C	0.151
C−O	0.139
C−H	0.109
O−H[b]	0.097
O_w−H_w	0.1
H_w−H_w[c]	0.163

Bonded Interactions: Bends

bend	θ°[deg]	k^a [kJ/(mol rad^2)]
C−C−H	109.49	359.996
H−C−H	108.30	322.322
C−C−O	109.04	719.992
O−C−H	110.07	468.832
C−O−C	111.56	623.714
C−O−H[b]	105	320

Bonded Interactions: Torsions

torsion	P	φ° [deg]	k^t [kJ/mol]
O−C−C−O	1	0	0.2093
	2	0	−10.6743
C−O−C−C	1	0	−4.1860
	2	0	−2.9302
	3	0	−1.3395
H−C−C−H	3	0	−1.1721
O−C−C−H	3	0	−1.1721
C−O−C−H	3	0	−3.3907
H−O−C−C[b]	3	180	2
H−O−C−H[b]	3	60	2

[a] The subscript "w" indicates that the atom pertains to a water molecule. In the SPC/E model for water, only O_w atoms are considered as Lennard-Jones interaction sites. [b] Adapted from a force field for poly(vinyl alcohol) in water.[20] [c] In the SPC/E model, a bond is considered between H_w atoms of the same molecule in order to keep the angle fixed.

implicitly for the effect of water molecules on the chain structure in a mean-field way, although they are not explicitly considered in the coarse-grained model.

3. Results and Discussion

3.1. Structural Properties of a Single PEO Chain in Aqueous Solution. The first step for the establishment of a coarse-grained model of PEO chains in water is the validation of the atomistic model used as basis for it. Table 3 shows the values of solution density and radii of gyration obtained from simulations of PEO chains with 10 repeat units and different terminal groups. Results indicate that the terminal group of the PEO chain does not have a significant influence on the size of the polymer chain in solution and that there is a good agreement between simulations and values extracted from experiments. At the values of molecular weight and temperature investigated here, PEO is completely soluble in water.[22]

For a more detailed picture of the chain structure, local conformations along the PEO chains were classified based on triads of torsional angles involving carbon and oxygen atoms along O−C−C−O segments. Here, we adopted the convention that the torsional angle is 0° for a fully eclipsed (cis) conformation and increased clockwise up to 180° (or decreased counterclockwise to −180°), reaching then a perfect trans conformation. Torsional angles were classified as trans (T) for $120° < |\varphi| \leq 180°$. Analogously, gauche (G) conformations were represented either as G^+ for $0° \leq \varphi \leq 120°$ or G^- for $-120° \leq \varphi < 0°$ (absence of the superscript denotes any gauche conformation). Figure 3 shows the population of different conformers in CH_3-terminated and H-terminated PEO chains. In the case of H-terminated chains, terminal O−C−C−O segments were neglected. The results demonstrate that the terminal groups of the PEO chain have only a minor influence on the distribution of conformational states, even for short chains with only 10 repeat units. Figure 3 shows that 90% of the torsions around C−C bonds are gauche. This preference for the gauche conformation, also known as the "gauche effect", is well-known in literature for PEO and DME in condensed phases.[15,23,24] Figure 3 also shows that the results agree fairly well with previous simulations and with the experimental behavior of DME, which can be regarded as a building motif of PEO chains.[15,17]

Table 2. Gaussian Bonded Parameters of Coarse-Grained Force Field

Bond Length Distribution

m	i	A_i	w_i [Å]	l_{ci} [Å]
2	1	0.915 93	0.237 49	2.876 95
	2	0.082 81	0.090 24	3.568 49

Angle Distribution

m	i	A_i	w_i [deg]	θ_{ci} [deg]
3	1	0.131 81	14.910 15	118.689 51
	2	0.857 81	28.059 67	150.015 48
	3	0.020 63	3.472 37	177.196 43

Figure 4 depicts the RDF of oxygen atoms along the backbone of an H-terminated PEO chain with 20 repeat units. The RDF was defined as the atom density at a given distance from a reference oxygen atom divided by the total system density. It exhibits two very pronounced peaks at 0.29 and 0.36 nm, which reflect the gauche and trans conformations of oxygen atoms in a O−C−C−O segment, respectively (see the correspondent Newman projections in Figure 4). At higher distances, the RDF still exhibits a structure with peaks that are however less pronounced.

3.2. Coarse-Graining of a PEO Chain. In the mapping of coarse-grained chains according to Figure 1, no distinction was made between CH_3-terminated and H-terminated PEO because the terminal group plays a minor role on the chain structure, as demonstrated in the previous section. For the establishment of interaction potentials in the coarse-grained model, the RDF of the oxygen atoms for a PEO chain with 20 monomers in water (see Figure 4) was adopted as target function. Figure 5a,b shows a comparison between the distribution of bond lengths and angles in the atomistic

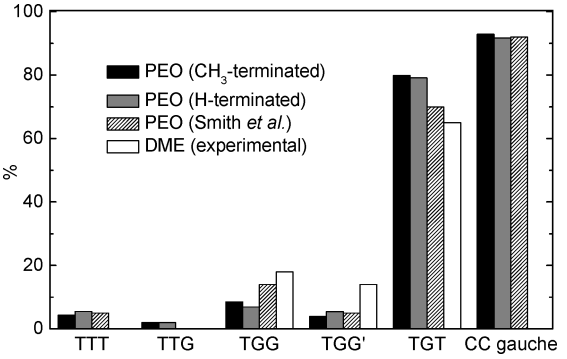

Figure 3. Population of conformers of CH_3-terminated and H-terminated PEO chains in aqueous solutions. Simulation results of the present work are compared to previous simulations of Smith et al. and with experimental results for DME found in the literature.[15,17]

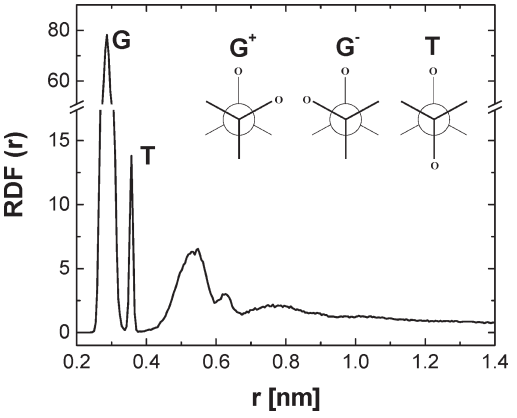

Figure 4. Radial distribution function of O atoms in the backbone of a single H-terminated PEO chain with 20 repeat units in aqueous solution. Inset shows Newman projections of an O−C−C−O segment with either gauche (G) or trans (T) conformation.

Table 3. Solution Properties and Radii of Gyration of PEO (10-mer) in Aqueous Solution

	solution density at 318 K [kg m^{-3}]		radius of gyration [nm]	
terminal group	simulation	experiment	simulation	experiment
$-CH_3$	991.23	~990.28[a]	0.63	0.5−0.7[b]
−H	991.99	~990.28[a]	0.61	−

[a] Approximated as the density of pure water, since solutions are dilute. [b] Extrapolation of experimental results.[17]

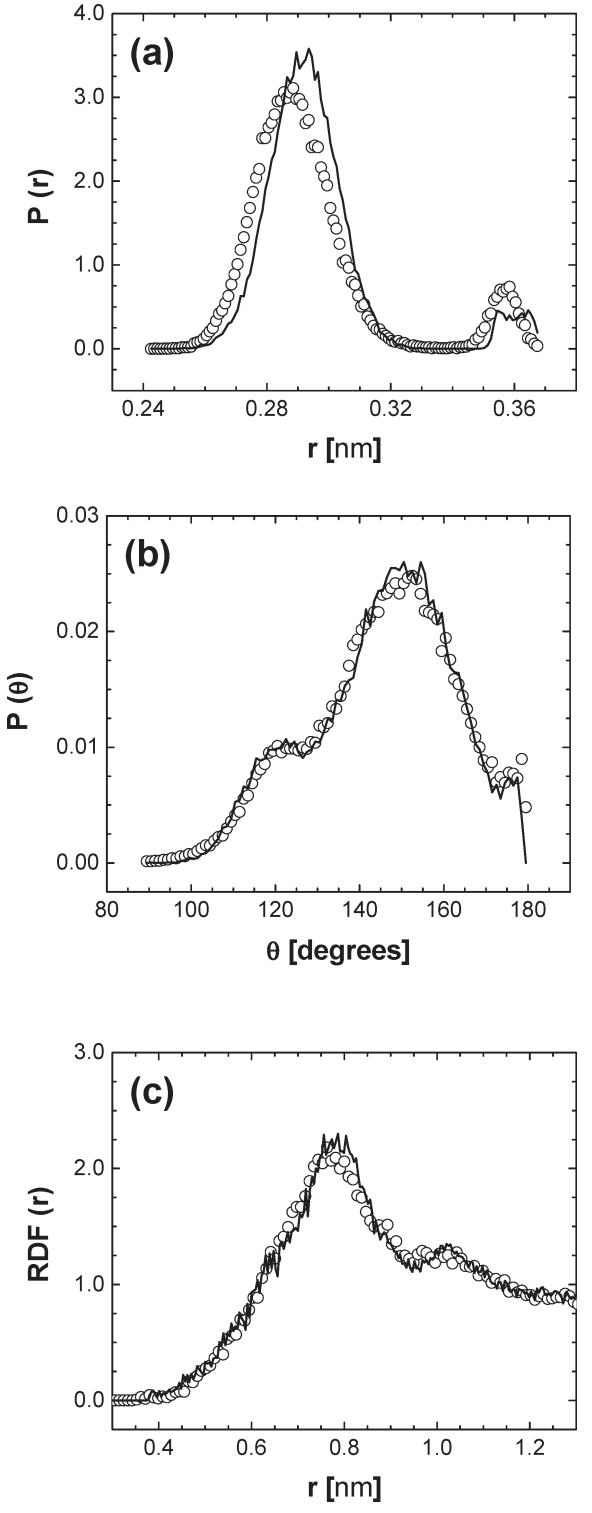

Figure 5. Structural properties of a single H-terminated PEO chain with 20 repeat units in aqueous solution (circles) used as targets for the elaboration of bonded and nonbonded potentials for the coarse-grained model (lines). (a) Distribution of bond distances between superatoms. (b) Distribution of angles (normalized by sin θ).[8] (c) Radial distribution function of superatoms separated by at least two other superatoms.

and coarse-grained model and Table 2 lists the fitting parameters of the Gaussian functions from Boltzmann inversion.

For nonbonded interactions, the process of iterative Boltzmann inversion using the RDF in Figure 5c as target resulted in the potential depicted in Figure 6. The potential derived from the coarse-graining process is a tabulated

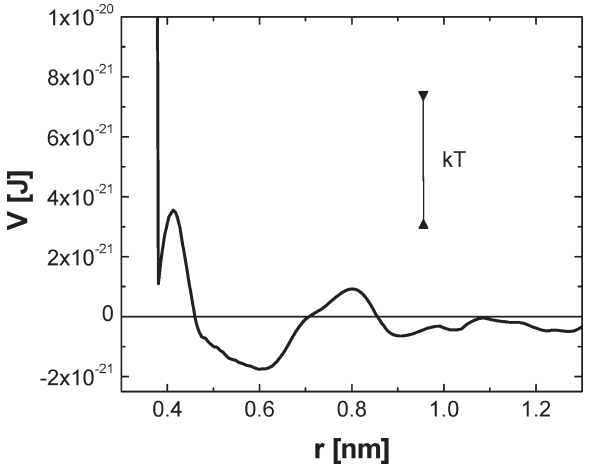

Figure 6. Nonbonded potential between superatoms as obtained by iterative Boltzmann inversion with the radial distribution function in Figure 5c as target. The vertical line represents the magnitude of the thermal energy kT.

potential and does not have an analytical form. The potential between superatoms exhibits an oscillatory profile with alternating regions of attraction and repulsion. Oscillations in the value of the potential become more pronounced as the distance between superatoms decreases, with the deepest potential well at 0.6 nm. The steep increase in the potential at shorter distances reflects the strong repulsion that prevents interpenetration between two superatoms. The potential in Figure 6 agrees qualitatively with results of Fischer et al. for shorter coarse-grained PEO chains in aqueous solution.[9] The use of the nonbonded interaction in Figure 6 in simulations generates chains with a RDF that closely matches the RDF of the original chain, as shown in Figure 5c.

3.3. Forces between Surfaces with Grafted Chains. After building the coarse-grained force field, we studied the force acting between parallel surfaces covered by coarse-grained PEO chains. Surfaces were pictured as a continuum, and the interaction of a superatom with the surface was described as a function of the distance z to the surface by:

$$V_i^{\text{surface}}(z) = \frac{C_R}{z^{10}} - f\frac{C_A}{z^6} \tag{7}$$

where the first term with the constant C_R describes the repulsive part of the potential and the second term with C_A describes the attractive part. This potential is smoother than the usual Lennard-Jones potential and therefore more appropriate to describe interactions between polymers and surfaces. It has been previously applied for the simulation of polymers on carbon surfaces.[25] Two different kinds of interactions were studied. In the first case, the constants C_R and C_A were taken as 4.48×10^{-25} J nm^{10} and 2.0×10^{-22} J nm^6, respectively, and the factor f as 1. The resulting potential was labeled as ATT-REP and exhibited a pronounced energy minimum, meaning a strong interaction between polymer and surface. In the second case, the values of the constants were taken as before except for f, that was set to 0 so that the resulting potential was purely repulsive and labeled as REP. Both potentials are valid qualitatively and are compared in Figure 7. Direct van der Waals interactions between the two surfaces were neglected.

In total, 25 chains were placed on each surface in a square array, each one bearing n monomers that interacted with the surface according to the potential in eq 7. Additionally, each

chain had an anchoring monomer firmly attached to the surface by harmonic potentials in all Cartesian directions so that they had an amplitude of vibration on the order of 0.3 Å. These anchor groups model either chemical bonds between polymer and surface or even strongly adsorbed head groups of the chains. The anchoring points were placed at opposite positions at both surfaces so as to provide a maximum overlap between opposing chains, as depicted in Figure 2. Grafting densities were varied in the interval between 0.01 and 2.44 chains/nm^2 by changing the lateral dimensions of the systems. Simulations were performed for different separation distances between the surfaces, varying between 3 and 18 nm. First, systems were equilibrated for 0.25 ns, followed by data acquisition for the same period of time. The mean force between the surfaces was calculated by averaging the instantaneous interaction forces between all superatoms (including the anchor monomers) and the surface.

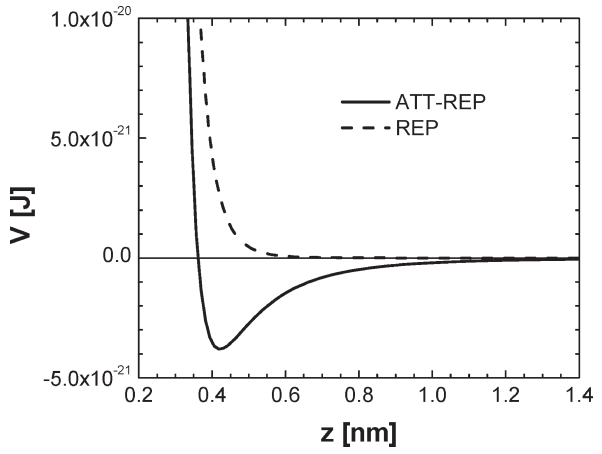

Figure 7. Different interaction potentials between elements of the coarse-grained chains and the surfaces, as given by eq 7 for purely repulsive surfaces (dashed line) or surfaces with an attractive and a repulsive term in the potential (full line).

Figure 8 shows density profiles of coarse-grained chains in the direction perpendicular to the surfaces for systems of chains with 12 repeat units and with different grafting densities. Distributions were smoothed over a distance of approximately 0.14 nm in order eliminate fine structures inherent in the coarse-grained model and to make the results comparable to those from atomistic simulations.[26] In a coarse-grained model, a whole monomer is pictured as a single bead, with the mass concentrated at its center.

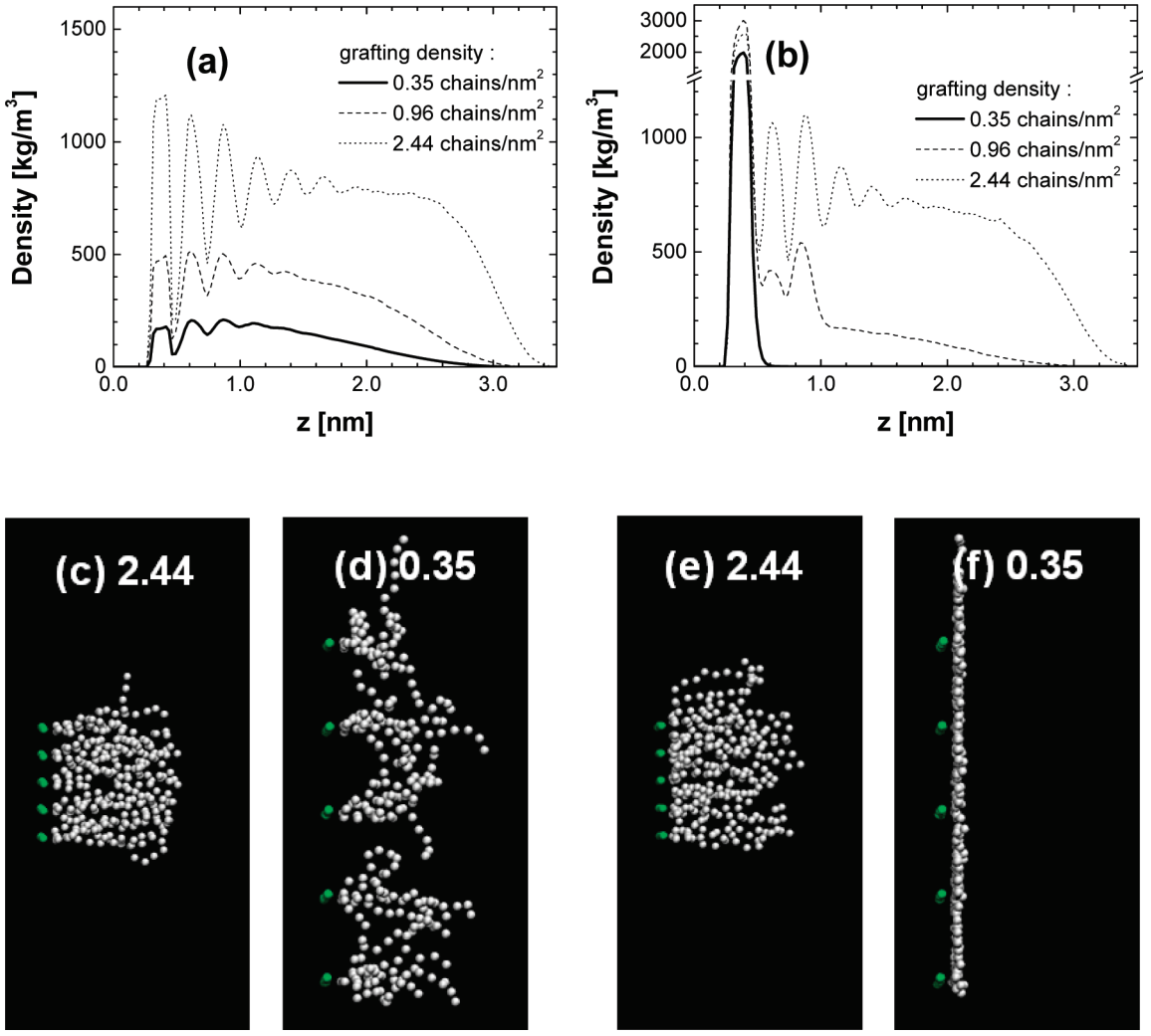

Figure 8. Smoothed density profiles of grafted coarse-grained chains with 12 repeat units. Distributions were recorded along the direction perpendicular to the surfaces for different grafting densities and with the (a) REP and (b) ATT-REP interactions between polymer and surfaces. The corresponding snapshots are also shown for the (c,d) REP and (e,f) ATT-REP interactions (numbers on top are the grafting density in chains/nm^2). White beads represent chain repeat units and green beads represent anchoring monomers at the surface (surface is not represented here).

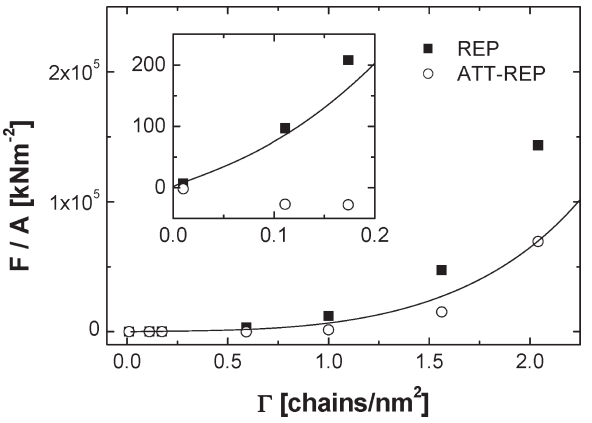

Figure 9. Force per unit area (area of both surfaces summed up) as a function of grafting density for different interactions between polymer and surfaces. Results were recorded for chains with 12 repeat units and a separation of 4 nm between surfaces. Inset shows an expansion of the region corresponding to lower grafting densities. Symbols are the results from simulations and full lines represent functions built based on eq 8.

The "concentration" of the mass of all monomer atoms at a single point in space leads to these fine structures in the density distributions. In the case of surfaces with a REP potential, the density profiles indicate that chains have an extended conformation and form a brush-like structure for all grafting densities Γ investigated. However, strong adsorption takes place on surfaces with the ATT-REP potential, as indicated by the well-defined peak at 0.38 nm in all the density profiles. For the case of low grafting densities, there is a large surface area available for adsorption and the system turns into a monolayer of adsorbed chains. As the grafting density increases, less area is available for adsorption and chains exhibit more extended conformations. Density distributions still show a very pronounced peak at 0.38 nm due to adsorption, but a considerable fraction of repeat units populate the aqueous media, so that the structure of the chains qualitatively resembles that of a brush. These trends agree with previous results obtained by means of atomistic simulations of PEO on graphite surfaces[26] and Monte Carlo simulations of the interaction between coated nanoparticles.[6] They show that, for the case of polymers with a strong affinity for the surface, high grafting densities are needed so that chains can achieve the structure of a brush. This has serious implications on colloid stability, because steric stabilization of particles covered by grafted polymer chains is more effective if these chains are able to extend themselves into the solution.

The influence of the grafting density and adsorption on the force between surfaces is illustrated in more detail in Figure 9. It shows that, for the case of surfaces with REP potential, the repulsion between the walls increases as the grafting density increases. This is due to both the higher number of chains per area and the more extended chain conformations expected for higher grafting densities. For surfaces with the ATT-REP potential, the repulsive force between surfaces is lower than the previous case because chains tend to adsorb at the surfaces and are less extended. The force becomes significant at grafting densities above 1 chain/nm^2. At lower grafting densities, however, the surface area available for adsorption for each chain is bigger and a considerable fraction of polymer segments is adsorbed, causing the force between surfaces to be negligible.

Figure 10 illustrates how the repulsive force between surfaces increases as a function of distance at for the REP potential, low grafting densities and for different chain

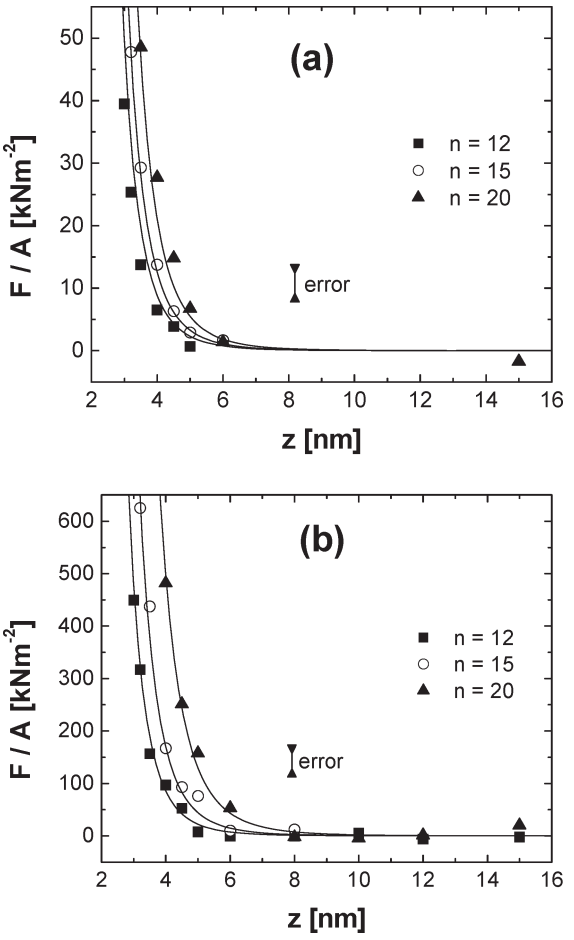

Figure 10. Force per unit area as a function of surface separation for chains with different number of repeat units n and for grafting density of (a) 1.0×10^{-2} and (b) 1.1×10^{-1} chains/nm^2. Symbols represent simulation results and full lines are functions generated based on eq 8. The magnitude of the error is indicated by vertical arrows. The interaction between monomers and surface is purely repulsive (REP).

lengths. The force increases monotonically as the distance decreases, in qualitative agreement with experimental measurements.[27−29] We found empirically that the behavior of the force can be expressed by a dependence on z^{-6}. For grafting densities lower than 0.2 chains/nm^2 and chain lengths in the range investigated, we found empirically that the dependence of the force on the distance between surfaces, grafting density and number of repeat units can be approximated by the general equation

$$\frac{F}{A} = \alpha[1 - \exp(\beta n^{0.8}\Gamma^{0.37})]z^{-6} \qquad (8)$$

where α and β are constants with values of -1.1627×10^{-50} kN m^4 and 1.064 nm$^{0.74}$, respectively. Equation 8 agrees satisfactorily with simulation results, as demonstrated in Figures 9 and 10. It respects the necessary boundary conditions that (1) the force tends to infinity as the distance between surfaces tends to 0 and (2) the force tends to 0 as the number of monomers per chain or the grafting density tend to 0.

For the case of higher grafting densities, the dependence of the force on z^{-6} is maintained, as shown in Figure 11. The use of ATT-REP potential decreases the force between the surfaces, but it is still significant because the area available for chain adsorption is small so that chains are able to have an extended conformation.

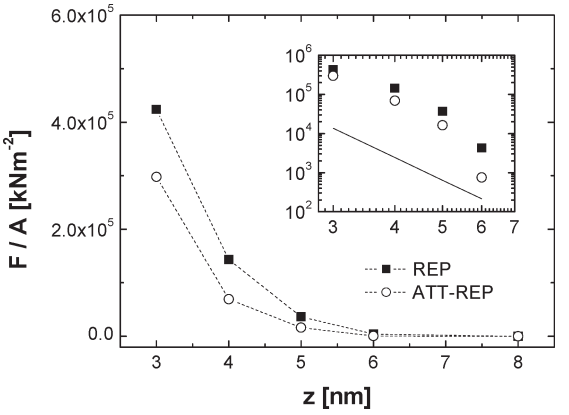

Figure 11. Force as a function of distance for chains with 12 repeat units, grafting density of 2.04 chains/nm^2 and different interactions between polymer and surface. Inset shows a double logarithmic plot of the same simulation results (symbols) compared with a straight line with slope 6, which indicates a linear dependence of the force on z^{-6}.

3.4. Model Applicability and Limitations. Within its applicability range, eq 8 may be used to predict the stability of colloidal particles covered by PEO chains in aqueous solutions. The energy per unit area of two approaching particles can be calculated by integrating eq 8 over distance, so that:

$$\frac{E(z)}{A} = -\int_{\infty}^{z} \frac{F(z')}{A}\,dz' = \frac{\alpha[1-\exp(\beta n^{0.8}\Gamma^{0.37})]}{5A} z^{-5} \qquad (9)$$

Figure 12a illustrates how the energy per unit area estimated by means of eq 9 varies as the surfaces of two particles approach each other. Energies are compared with the average thermal energy kT for the case of different cross sectional areas of contact. It shows that the approximation of particles (that may eventually lead to aggregation) costs more energy in the case of longer chains and higher grafting densities.

Figure 12b compares the energy curves for two systems. The first system is characterized by $n = 12$ and $\Gamma = 0.183$ chains/nm^2, and the second by $n = 20$ and $\Gamma = 0.11$ chains/nm^2. Although both systems have the same number of repeat units per unit area (i.e., 0.22 units/nm^2), the stabilization effect is higher in the system with higher molecular weight. This is consistent with the fact that the dependence of the energy on n is more pronounced than the dependence on Γ, according to eq 9. This means that, for the same mass of polymeric material spent as additive, chains with higher molecular weight lead to a more effective stabilization.

The model developed here does not consider van der Waals interactions between the surfaces but these can be to a good approximation simply added to the results analytically. In the context of a DLVO model, for instance, consideration of eq 9 would account for an extra activation energy for particle aggregation due to entropic effects related to the mechanism of steric stabilization by grafted polymer chains.

An additional effect that may be relevant is the contribution of osmotic pressure to the force profiles.[29,30] As two surfaces come closer to each other in experiments, water is expelled from the gap and the local polymer concentration increases. However, accounting for the effect of osmotic pressure on the simulations performed here is not trivial, since water molecules are not explicitly considered.

4. Conclusions

We performed atomistic molecular dynamics simulations of CH_3-terminated and H-terminated PEO chains in aqueous solutions. Atomistic results show that structural properties such as the chains' radius of gyration and conformer distributions do not depend on the terminal group and are consistent with experimental results. It was found that successive O atoms along the backbone are preferably at gauche conformation, in agreement with previous simulations and experimental results, thus providing several validations of the atomistic force field used.

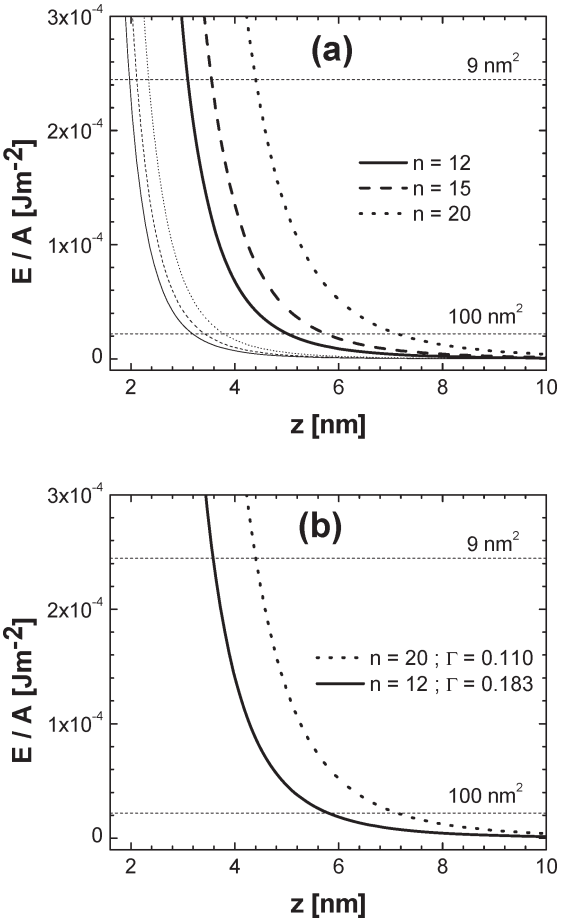

Figure 12. Energy per unit area of two parallel surfaces as a function of the distance between surfaces, as calculated by means of eq 9. Results are compared to the value of the thermal energy kT per unit area for different values of cross sectional area (horizontal dashed lines). (a) Comparison between chains with different number of repeat units n at grafting densities of 1.0×10^{-2} (thin lines) and 1.1×10^{-1} (bold lines) chains/nm^2. (b) Comparison between chains with different n and grafting densities Γ (given in chain/nm^2), keeping in both cases the same amount of material (i.e., 0.22 repeat units/nm^2).

On the basis of the chain structure obtained from atomistic simulations, we successfully constructed a coarse-grained model of PEO chains in aqueous solution, in which each repeat unit of the original chain was mapped by an individual superatom centered at an O atom from the backbone. Water molecules were not explicitly considered. Their influence on chain structure was rather incorporated in the coarse-grained nonbonded interactions, considerably increasing the computational efficiency.

The force between parallel surfaces with grafted coarse-grained chains was calculated as a function of surface separation (3−18 nm), number of elements in each chain (12−20), and grafting density (0.01−2.04 chains/nm^2). Repulsive forces increase monotonically as surfaces come closer, in qualitative agreement with experimental results.

The impact of the interaction between polymer and surface was investigated by means of two representative cases. In the first,

a purely repulsive interaction was considered between surface and polymer, and in the second, a surface with high affinity for the polymer was taken. It was shown that, in the case of purely repulsive surfaces, chains have an extended conformation that leads to a higher force between surfaces and consequently to a more effective particle stabilization. For surfaces with higher affinity for the polymer, some adsorption takes place. The polymer structure is strongly dependent on the grafting density. At low grafting densities, a large area is available for adsorption and the chain repeat units may form in the extreme case a monolayer over the surface, leading to poor particle stabilization. As the grafting density increases, less area is available for adsorption and chains have more extended conformations resembling a brush. In this regime, the repulsive force between surfaces is significant in spite of the high affinity between polymer and surface.

Finally, it has been shown that the chain molecular weight has a more pronounced influence on particle stability than the grafting density. Comparing two systems with different molecular weights and grafting densities, but keeping the mass of polymeric material per unit area the same, a stronger stabilization effect is observed for systems with higher molecular weight.

Acknowledgment. We thank Frederic Leroy and Hossein Ali Karimi for fruitfull discussions regarding the simulation method.

References and Notes

(1) Douillard, J. M.; Pougnet, S.; Faucompre, B.; Partyka, S. J. *Colloid Interface Sci.* **1992**, *154*, 113.
(2) Nevskaia, D. M.; Sepulveda-Escribano, A.; Guerrero-Ruiz, A. *Phys. Chem. Chem. Phys.* **2001**, *3*, 463.
(3) Murat, M.; Grest, G. S. *Macromolecules* **1989**, *22*, 4054.
(4) Murat, M.; Grest, G. S. *Phys. Rev. Lett.* **1989**, *63*, 1074.
(5) Meredith, J. C.; Sanchez, I. C.; Johnston, K. P.; de Pablo, J. J. *J. Chem. Phys.* **1998**, *109*, 6424.
(6) Duque, D.; Peterson, B. K.; Vega, L. F. *J. Phys. Chem. C* **2007**, *111*, 12328.
(7) Müller-Plathe, F. *ChemPhysChem* **2002**, *3*, 754.
(8) Milano, G.; Müller-Plathe, F. *J. Phys. Chem. B* **2005**, *109*, 18609.
(9) Fischer, J.; Paschek, D.; Geiger, A.; Sadowski, G. *J. Phys. Chem. B* **2008**, *112*, 13561.
(10) Smith, G. D.; Jaffe, R. L.; Yoon, D. Y. *J. Phys. Chem.* **1993**, *97*, 12752.
(11) Bedrov, D.; Pekny, M.; Smith, G. D. *J. Phys. Chem. B* **1998**, *102*, 996.
(12) Bedrov, D.; Borodin, O.; Smith, G. D. *J. Phys. Chem. B* **1998**, *102*, 5683.
(13) Bedrov, D.; Smith, G. D. *J. Chem. Phys.* **1998**, *109*, 8118.
(14) Bedrov, D.; Smith, G. D. *J. Phys. Chem. B* **1999**, *103*, 3791.
(15) Smith, G. D.; Bedrov, D.; Borodin, O. *J. Am. Chem. Soc.* **2000**, *122*, 9548.
(16) Smith, G. D.; Borodin, O.; Bedrov, D. *J. Comput. Chem.* **2002**, *23*, 1480.
(17) Fischer, J.; Paschek, D.; Geiger, A.; Sadowski, G. *J. Phys. Chem. B* **2008**, *112*, 2388.
(18) Müller-Plathe, F. *Comput. Phys. Commun.* **1993**, *78*, 77.
(19) www.theo.chemie.tu-darmstadt.de/group/services/yaspdoc/yaspdoc.html
(20) Müller-Plathe, F.; van Gunsteren, W. F. *Polymer* **1997**, *38*, 2259.
(21) www.theo.chemie.tu-darmstadt.de/ibisco/
(22) Bekiranov, S.; Bruinsma, R.; Pincus, P. *Phys. Rev. E* **1997**, *55*, 577.
(23) Müller-Plathe, F.; van Gunsteren, W. F. *Macromolecules* **1994**, *27*, 6040.
(24) Müller-Plathe, F. *Acta Polym.* **1994**, *45*, 259.
(25) Daoulas, K. C.; Harmandaris, V. A.; Mavrantzas, V. G. *Macromolecules* **2005**, *38*, 5780.
(26) Bedrov, D.; Smith, G. D. *Langmuir* **2006**, *22*, 6189.
(27) Kuhl, T. L.; Leckband, D. E.; Lasic, D. D.; Israelachvili, J. N. *Biophys. J.* **1994**, *66*, 1497.
(28) Drobek, T.; Spencer, N. D.; Heuberger, M. *Macromolecules* **2005**, *38*, 5254.
(29) Kenworthy, A. K.; Hristova, K.; Needham, D.; McIntosh, T. J. *Biophys. J.* **1995**, *68*, 1921.
(30) Hansen, P. L.; Cohen, J. A.; Podgornik, R.; Parsegian, V. A. *Biophys. J.* **2003**, *84*, 350.